

# Optimization and Configuration of Control Parameters to Enhance Small-signal Stability of Hybrid LCC-MMC HVDC System

Chunyi Guo, Peng Cui, and Chengyong Zhao

**Abstract**—This paper investigates the small-signal stability of the hybrid high-voltage direct current (HVDC) transmission system. The system is composed of line commutated converter (LCC) as rectifier and modular multi-level converter (MMC) as inverter under weak AC grid condition. Firstly, the impact of short-circuit ratio (SCR) at inverter side on the system stability is investigated by eigen-analysis, and the key control parameters which have major impact on the dominant mode are identified by the participation factor and sensitivity analysis. Then, considering the quadratic index and damping ratio characteristic, an objective function for evaluating the system stability is developed, and an optimization and configuration method for control parameters is presented by the utilization of Monte Carlo method. The eigenvalue results and the electromagnetic transient (EMT) simulation results show that, with the optimized control parameters, the small-signal stability and the dynamic responses of the hybrid system are greatly improved, and the hybrid system can even operate under weak AC grid condition.

**Index Terms**—Hybrid high-voltage direct current (HVDC), line commutated converter (LCC), modular multi-level converter (MMC), optimization of control parameter.

## I. INTRODUCTION

**L**INE commutated converter based high-voltage direct current (LCC-HVDC) transmission has been widely used in long-distance bulk power transmission and asynchronous grid interconnection [1]. However, there are also some operation problems, especially when connecting weak AC grid such as overvoltage, commutation failure, and small-signal instability [2]–[6].

Recently, modular multi-level converter (MMC) scheme has become a more promising option for practical application of voltage source converter based HVDC (VSC-HVDC) technology, owing to its advantages such as modularity, less harmonics, lower switching losses, and no commutation fail-

ures [7]–[10].

LCC-MMC HVDC system combines the advantages of LCC and MMC technology, and has a potential for practical application [11]. Nowadays, State Grid Corporation of China (SGCC) and China Southern Power Grid (CSG) both plan to upgrade some of the existing LCC-HVDC links as hybrid HVDC to effectively mitigate the potential cascaded commutation failures. In May 2018, CSG started the construction of Wudongde hybrid three-terminal HVDC project, where a  $\pm 800$  kV/8000 MW LCC station in Yunnan Province is the rectifier, and two  $\pm 800$  kV MMCs in Guangdong Province and Guangxi Province are inverters with capacities of 5000 MW and 3000 MW, respectively [12].

Existing literature related to the hybrid LCC-MMC HVDC system mainly focuses on the operation characteristics [13], [14], coordinated control method [15], [16], dynamic responses under fault conditions [17], [18], etc. Small-signal stability analysis is required in systematic control design and dynamic performance evaluation, and the stability margin can be improved by the optimization and configuration of control parameters. Reference [19] presents a small-signal model of a hybrid multi-terminal DC network. However, the internal harmonics of MMC and the phase-lock-loop (PLL) dynamics are not considered. Reference [20] presents the small-signal stability of the hybrid LCC-MMC HVDC system, and the results show that the system may experience instability issue under weak AC grid condition. However, the mitigation method for instability issue is not involved and needs further research. The system stability could be improved by optimizing the control parameters [21]–[23]. However, the dynamic responses are not always considered in the optimization process.

This paper proposes an effective optimization and configuration method for control parameters to improve the small-signal stability and dynamic responses of the hybrid LCC-MMC HVDC system. Based on the derived small-signal model, the impact of AC system strength on the stability of the hybrid LCC-MMC HVDC system is investigated, and the dominant mode is obtained which may cause system oscillation. Then, an objective function considering the quadratic index and damping ratio characteristic is developed, and an optimization and configuration method for control parameters is presented by Monte Carlo method. The results show that the optimized control parameters can improve the small-signal stability of the system, the dynamic response charac-

Manuscript received: June 5, 2020; revised: August 16, 2020; accepted: September 14, 2020. Date of CrossCheck: September 14, 2020. Date of online publication: February 9, 2021.

This work was supported by the National Natural Science Foundation of China (No. 51877077).

This article is distributed under the terms of the Creative Commons Attribution 4.0 International License (<http://creativecommons.org/licenses/by/4.0/>).

C. Guo (corresponding author), P. Cui, and C. Zhao are with the School of Electrical Engineering, North China Electric Power University, Beijing 102206, China (e-mail: chunyi guo@gmail.com; cuipeng467@163.com; chengyong-zhao@ncepu.edu.cn)

DOI: 10.35833/MPCE.2020.000354



teristics and even fault recovery performance of the LCC-MMC system when connected to weak AC grid.

The rest of the paper is organized as follows. Section II presents the hybrid LCC-MMC HVDC system. Section III introduces the small-signal dynamic model for the hybrid LCC-MMC HVDC system. Section IV analyzes the system stability under weak AC grid condition. Section V identifies the key control parameters by the method of participation factor and parametric sensitivity analysis. Section VI derives the objective function considering the quadratic index and damping ratio characteristic. Section VII optimizes the control parameters by Monte Carlo method and validates the effectiveness of the proposed method. Finally, Section VIII concludes the paper.

## II. HYBRID LCC-MMC HVDC SYSTEM

### A. System Configuration

The system is a 2000 MW,  $\pm 500$  kV bipolar hybrid LCC-MMC HVDC link with positive pole as shown in Fig. 1(a), which is composed of an LCC station connected to an AC system 1 through AC filter and a converter transformer as well as an MMC station connected to AC system 2 through a transformer. Figure 1(b) shows the equivalent circuit of the system. The AC filter configuration of LCC is that of CI-GRE Benchmark model [24]. The system parameters in Fig. 1 are given in Appendix A Table AI.

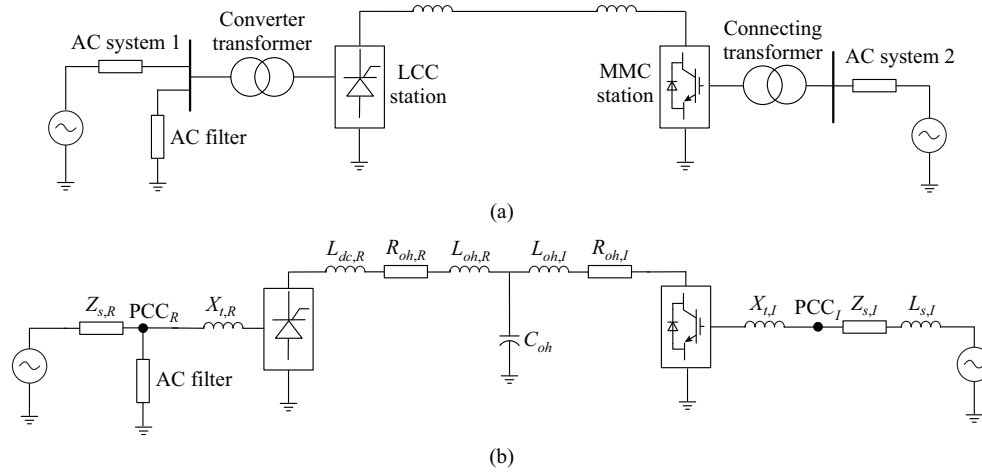


Fig. 1. Hybrid LCC-MMC HVDC system. (a) Schematic diagram. (b) Equivalent circuit of system.

### B. Control System for Hybrid LCC-MMC HVDC System

The control system for the hybrid LCC-MMC HVDC system is shown in Fig. 2. The conventional PLL for LCC (PLL1) of Fig. 2(a) is in synchronism with positive-sequence voltage. The constant DC current control for LCC of Fig. 2(b) is utilized in LCC station to generate the advancing firing angle  $\beta$  through a proportional integral (PI)

function. The circulating current suppression controller (CC-SC) is shown in Fig. 2(c). The conventional PLL of Fig. 2(d) (PLL2) keeps the MMC in synchronism with positive-sequence voltage. The vector current control (VCC) of Fig. 2(e) is adopted for MMC to adjust the voltage at DC side and AC side. The control parameters of Fig. 1 are given in Appendix A Table AI and Table AII.

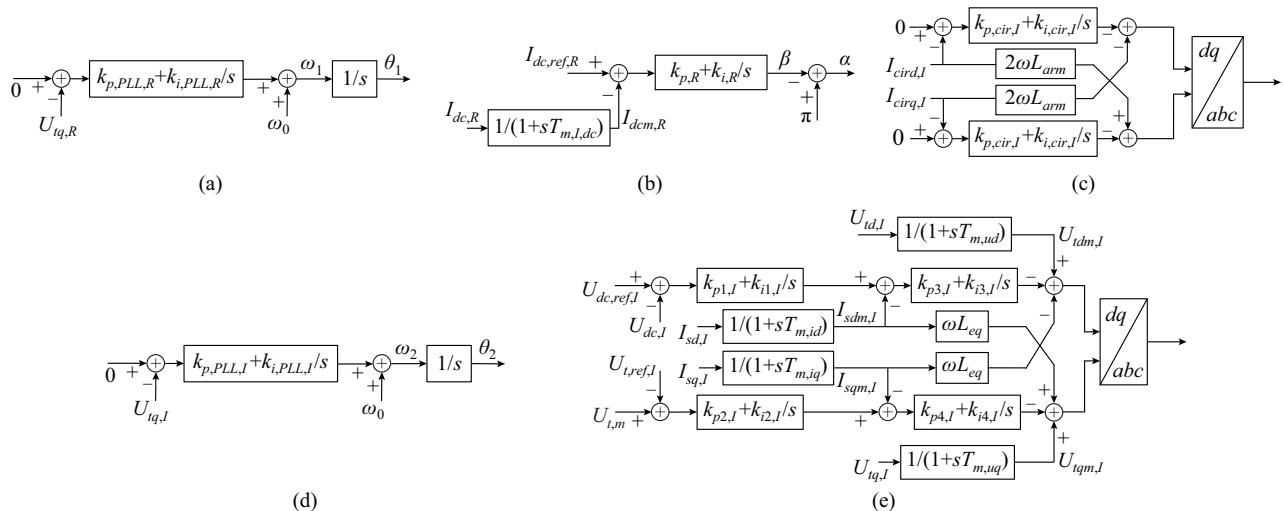


Fig. 2. Control system for hybrid LCC-MMC HVDC system. (a) PLL1 for LCC. (b) Constant DC current control for LCC. (c) CCSC. (d) PLL2 for MMC. (e) VCC.

### III. SMALL-SIGNAL DYNAMIC MODEL

A non-linear state-space model of the hybrid LCC-MMC HVDC system is derived, including the dynamics of LCC station, MMC station and the control system. The detailed dynamic equations of LCC and MMC can be found in [20]. By linearizing the state-space model of the hybrid LCC-MMC HVDC system at an operation point, a 44-order small-signal dynamic model can be obtained as:

$$\frac{d\Delta X}{dt} = A\Delta X + B\Delta U \quad (1)$$

where  $\mathbf{X} = [U_{id,R}, U_{iq,R}, U_{cr2d,R}, U_{cr2q,R}, U_{cr3d,R}, U_{cr3q,R}, U_{cr4d,R}, U_{cr4q,R}, I_{Lr1d,R}, I_{Lr1q,R}, I_{Lr2d,R}, I_{Lr2q,R}, I_{sd,R}, I_{sq,R}, x_{1,R}, I_{dcn,R}, x_{2,R}, x_{PLL,R}, I_{dc,R}, U_{c,dc}, u_{c,dc,I}, u_{cRd,I}, u_{cRq,I}, u_{cld,I}, u_{clq,I}, u_{c3x,I}, u_{c3y,I}, I_{cd,I}, I_{sd,I}, I_{sq,I}, I_{cird,I}, I_{cirq,I}, I_{smd,I}, I_{sqm,I}, U_{tdm,I}, U_{uqm,I}, x_{1,I}, x_{2,I}, x_{3,I}, x_{4,I}, x_{5,I}, x_{PLL,I}, f_{1,I}, f_{2,I}]^T$  is the state-variable vector;  $\mathbf{U} = [U_{dc,ref,R}, U_{dc,ref,I}, U_{t,ref,I}]^T$  is the input vector, and  $I_{dc,ref,R}, U_{dc,ref,I}, U_{t,ref,I}$  are the reference values of DC current of LCC, the DC and AC voltage of MMC, respectively;  $\mathbf{A}$  is the state matrix; and  $\mathbf{B}$  is the input matrix of the small-signal dynamic model. The specific physical meaning can be found in Appendix A Table AII.

#### IV. ANALYSIS OF SMALL-SIGNAL STABILITY FOR HYBRID LCC-MMC HVDC SYSTEM UNDER WEAK AC GRID CONDITION

One major advantage of the hybrid LCC-MMC HVDC system is its ability to deliver the power to weak or even passive network. However, recent literature shows that, weak AC grid or lower short-circuit ratio (SCR) may lead to system instability [6], [20]. This section evaluates the impact of the receiving AC system strength  $SCR_2$  on the stability of the hybrid LCC-MMC HVDC system, and calculates the critical  $SCR_2$  that the system can tolerate at the nominal operation point with initial control parameters.

Initially, the system operates at the nominal point of  $SCR_1 = 2.5$ ,  $SCR_2 = 2$ ,  $I_{dc,ref,R} = 1.0$  p.u.,  $U_{dc,ref,I} = 1.0$  p.u., and  $U_{t,ref,I} = 1.0$  p.u..  $SCR_1$  indicates AC system strength at LCC side,  $SCR_2$  indicates AC system strength at MMC side, and the AC system impedance angles at LCC side and MMC side are both  $85^\circ$ . Based on the small-signal model, Fig. 3 shows the root locus with  $SCR_2$  reducing from 2 to 1.

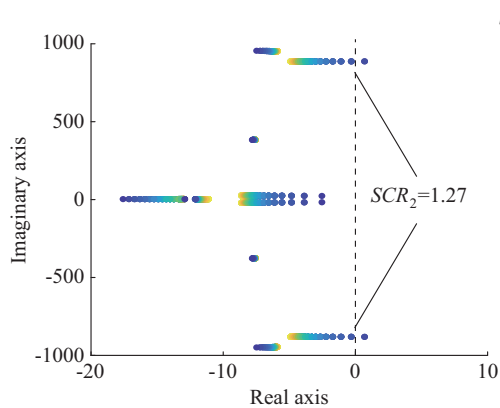


Fig. 3. Root locus with  $SCR_2$  reducing from 2 to 1.

The dominate mode of the system, i. e., the least-damped

mode for the nominal operation point, moves towards the right half plane as  $SCR_2$  reduces. Figure 3 shows that the critical  $SCR_2$  is 1.27. The system will be unstable when  $SCR_2$  is smaller than 1.27.

To validate the eigenvalue result of Fig. 3, Fig. 4 presents the simulation results with  $SCR_2$  reducing from 1.30 to 1.25. Initially,  $SCR_2$  is 1.30, then it is reduced to 1.25 when  $t = 5$  s. The DC current of LCC  $I_{dc,R}$  and DC voltage of MMC  $U_{dc,I}$  responses are shown in Fig. 4(a) and (b). Figure 4 illustrates that when  $SCR_2$  is reduced from 1.30 to 1.25, the system experiences instability, which verifies eigenvalue results of Fig. 3.

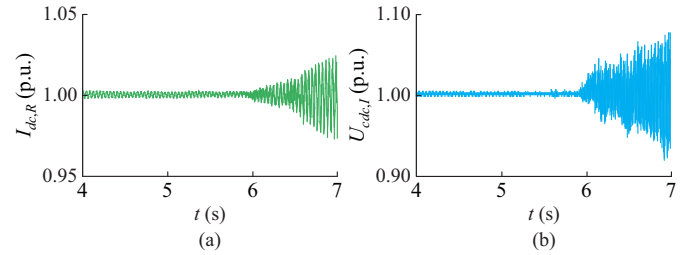


Fig. 4. Simulation results with  $SCR_2$  reducing from 1.30 to 1.25. (a) DC current of LCC. (b) DC voltage of MMC.

## V. ANALYSIS OF PARTICIPATION FACTOR AND PARAMETRIC SENSITIVITY

Based on the analysis of normalized participation factor [25], the most critical state-variables that participate in the dominate mode are recognized when  $SCR_2$  is 1.27 and 2.00, as shown in Fig. 5. All the state-variables of the system are divided into seven groups, i.e., LCC station, LCC AC system, LCC control, DC system, MMC station, MMC AC system, and MMC control. The major contributors of the state-variables have higher participation factors when  $SCR_2 = 1.27$  than  $SCR_2 = 2.00$ , which are  $x_{2,R}$  (related to LCC system),  $u_{dc,I}$  (related to DC side of MMC system),  $x_{3,I}$  (related to MMC control system) and  $x_{PLL,I}$  (related to PLL of MMC). On the contrary, the state variables  $f_{1,I}$  and  $f_{2,I}$  related to CCSC have lower participation factors when  $SCR_2$  is 1.27. Thus, the dynamics of the controllers described by these state-variables have major effects on the small-signal stability of the hybrid system.

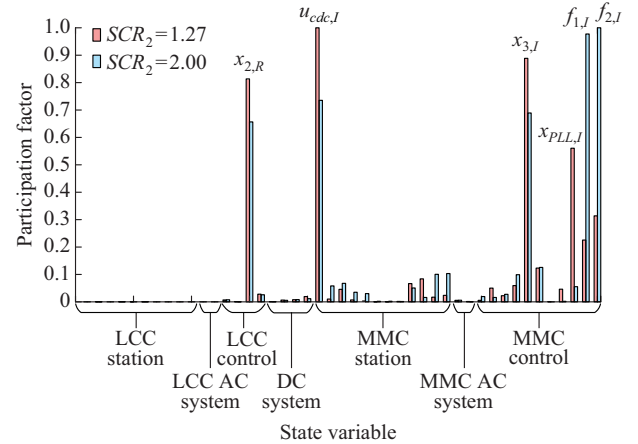


Fig. 5. Participation factor of hybrid system with different  $SCR_2$ .

To further investigate the effect of control parameters on

system stability, Fig. 6 compares the parametric sensitivity of the poorly damping modes (the damping ratio is less than 0.05) [26], [27] with the control parameters. In Fig. 6,  $\zeta$  is the damping ratio, and  $\zeta_1=0.09\%$ ,  $\zeta_2=0.08\%$ ,  $\zeta_3=3.33\%$ ,  $\zeta_4=3.91\%$ , and  $\zeta_5=0.01\%$ . In order to facilitate the observation, the sensitivity values are divided by the highest one of the group to obtain the normalized results.

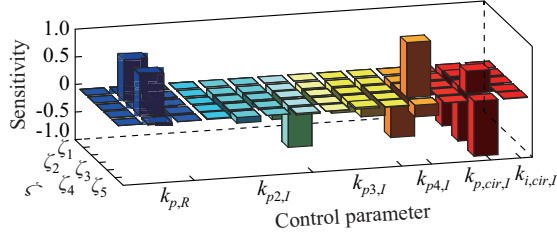


Fig. 6. Parametric sensitivity of poorly damping modes.

In Fig. 6, the key control parameters that have major impact on small-signal stability of the system are identified, which are constant DC-current controller gain  $k_{p,R}$  of LCC, VCC reactive outer-loop controller gain  $k_{p2,I}$  of MMC, inner-loop controller gains of  $d$ -axis and  $q$ -axis currents  $k_{p3,I}$  and  $k_{p4,I}$  for MMC, and the CCSC gains  $k_{p,cir,I}$  and  $k_{i,cir,I}$ . From Fig. 6, many control parameters have the impact on the system stability and their sensitivity values, i.e., magnitude and sign. Thus, the system stability could be enhanced by optimizing and configuring multiple control parameters.

## VI. OBJECTIVE FUNCTION FOR CONTROL PARAMETER OPTIMIZATION BASED ON QUADRATIC INDEX AND DAMPING RATIO CHARACTERISTIC

### A. Quadratic Index of Hybrid LCC-MMC HVDC System

Based on the derived small-signal dynamic model, the participation factor and parametric sensitivity for the hybrid LCC-MMC HVDC system, a quadratic index is derived to intuitively and quantitatively reflect the system stability.

A quadratic index  $J$  describing the small-signal stability is presented as:

$$J = \frac{1}{2} \int_0^\infty (\Delta \mathbf{x}(t) - \Delta \mathbf{X}_0)^T \mathbf{Q}_1 (\Delta \mathbf{x}(t) - \Delta \mathbf{X}_0) dt \quad (2)$$

where  $\Delta \mathbf{x}(t)$  is the state-variable deviation vector;  $\Delta \mathbf{X}_0$  is the initial value for  $\Delta \mathbf{x}(t)$  and  $\Delta \mathbf{X}_0 = \mathbf{0}$ ; and  $\mathbf{Q}_1$  is the weight coefficient matrix. In Section V, the obtained participation factors describe the effect of each state-variable in a specific dominant mode, which can be filled in the weight coefficient matrix accordingly to obtain  $\mathbf{Q}_1$ .

When the system is stable, the state variables will converge to a stable operation point, i.e.,  $\Delta \mathbf{x}(t) = \mathbf{0}$ , and the quadratic index  $J$  of (2) will be close to 0. The smaller the value of  $J$  is, the more stable the system will be. Therefore,  $J$  can be used as a reasonable evaluation index for small-signal stability of the system.

The outputs are given as:

$$\Delta \mathbf{y} = \mathbf{C} \Delta \mathbf{x}(t) \quad (3)$$

where  $\mathbf{C}$  is the output matrix of state-space equation.

For the hybrid LCC-MMC HVDC system shown in Fig. 1, some of the state-variables cannot be measured and ob-

tained in practical engineering. It is more practical to employ the quadratic sub-optimal index of output feedback to evaluate the system stability [28]. Hence, we utilize a low-dimensional output  $\Delta \mathbf{u}$  as control variables to form a feedback system as:

$$\Delta \mathbf{u} = -\mathbf{K} \Delta \mathbf{y} = -\mathbf{K} \mathbf{C} \Delta \mathbf{x}(t) \quad (4)$$

where  $\mathbf{K}$  is the output feedback coefficient matrix.

From [28], for an asymptotically stable system, the final form of the quadratic expression can be given as:

$$J = \frac{1}{2} \Delta \mathbf{x}^T(0) \mathbf{P} \Delta \mathbf{x}(0) \quad (5)$$

where the matrix  $\mathbf{P}$  can be obtained by:

$$(\mathbf{A} - \mathbf{B} \mathbf{K} \mathbf{C})^T \mathbf{P} + \mathbf{P} (\mathbf{A} - \mathbf{B} \mathbf{K} \mathbf{C}) = -\mathbf{Q}_1 \quad (6)$$

By solving matrix  $\mathbf{P}$  from (6),  $J$  can be calculated from (5).

The relationship between  $J$  and the hybrid system is shown in Fig. 7, and the dotted arrow indicates corresponding control loop. By integrating (5) and (6),  $J$  can be finally solved when  $\Delta \mathbf{x}(0)$  is a nominal value.

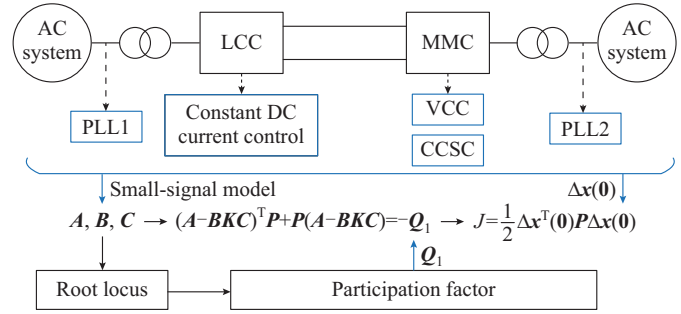


Fig. 7. Relationship between  $J$  and hybrid system.

From Fig. 7, by optimizing and configuring the control parameters, the matrices  $\mathbf{A}$ ,  $\mathbf{B}$ ,  $\mathbf{C}$  and  $\mathbf{Q}_1$  would change, thus  $J$  and the system stability would be different.

### B. Damping Ratio Characteristic of Hybrid LCC-MMC HVDC System

From [26], the poorly damping modes may cause system instability, i.e., the stability margin of the system can be reflected by the damping ratio to some extent. Thus, the damping ratio characteristic is also considered as the partial objective function to optimize the system control parameters.

The frequency  $f$  and the damping ratio  $\zeta$  of an oscillation mode are defined as:

$$\begin{cases} f = \frac{\omega}{2\pi} \\ \zeta = -\frac{\sigma}{\sqrt{\sigma^2 + \omega^2}} \end{cases} \quad (7)$$

From the eigenvalue analysis, when the root locus moves to right-half plane, the system becomes unstable, and the damping ratio of the dominant mode becomes negative. To comprehensively represent the damping ratio characteristics of the system, an average damping ratio  $D$  is presented as:

$$D = \sum_{i=1}^n \left| \frac{\zeta_i}{\zeta_{\min}} \right| \frac{\zeta_{\min}}{n} \quad (8)$$

where  $\zeta_i$  is the damping ratio of mode  $i$  ( $i=1, 2, \dots, n$ ); and

$\zeta_{\min}$  is the minimum damping ratio among  $n$  oscillatory modes at a specific operation point. Once the eigenvalue locus moves to right-half plane, i.e.,  $\zeta_{\min}$  is negative,  $D$  will also be negative and the hybrid system will experience the instability. Hence, only when all the damping ratios are positive, can the average damping ratio  $D$  be positive. Furthermore, the larger the value of  $D$  is, the wider the stability margin for the system will be.

### C. Objective Function

By integrating (2) and (8), the final objective function  $OBJ$  which describes the small-signal stability of the hybrid system is given as:

$$OBJ = k_1 J + k_2 \frac{1}{D} \quad (9)$$

where  $k_1$  and  $k_2$  are the contributions of quadratic index and damping ratio characteristics to the objective function, respectively. The values of  $k_1$  and  $k_2$  are in the range of  $[0, 1]$ , and  $k_1 + k_2 = 1$ . When the damping ratio of the hybrid system is relatively poor, i.e.,  $D$  is small,  $1/D$  in (9) will have a major influence on the objective function. On the contrary, if  $D$  is not small, while the cumulative amount of all the state-variable deviation is large,  $J$  in (9) will have a major influence. To ensure the universality,  $k_1 = k_2 = 0.5$ . The smaller  $OBJ$  is, the better stability for the hybrid system will be. If  $OBJ$  is negative or positive infinity, the hybrid system will become unstable.

### D. Impact of Control Parameters on Objective Function

We evaluate the effects of sensitive control parameters on the objective function under weak AC grid condition at the operation point of  $SCR_1 = 2.5$ ,  $SCR_2 = 1.27$ ,  $I_{dc,ref,R} = 1.0$  p.u.,  $U_{dc,ref,I} = 1.0$  p.u., and  $U_{i,ref,I} = 1.0$  p.u.. Based on the parametric sensitivity analysis, the highly sensitive control parameters  $k_{p,R}$  (constant current controller gain of LCC) and  $k_{p,cir,I}$  (CCSC gain of MMC) is taken as variables, the  $OBJ$  curve with varying  $k_{p,R}$  and  $k_{p,cir,I}$  is shown in Fig. 8. The highly sensitive control parameters, i.e.,  $k_{p,R}$  and  $k_{p,cir,I}$ , have a significant impact on the value of  $OBJ$ . And there exists a coupling effect between different parameters, i.e.,  $k_{p,cir,I}$  has different impacts on  $OBJ$  with  $k_{p,R}$  changing. Therefore, it is necessary to comprehensively consider the influence of both LCC and MMC control parameters on system stability.

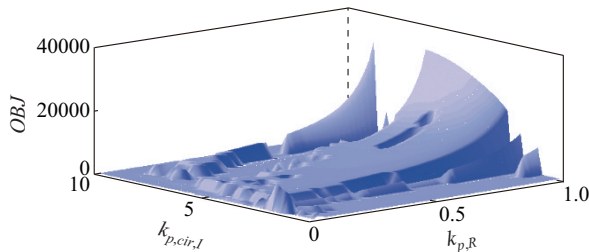


Fig. 8.  $OBJ$  curve with varying  $k_{p,R}$  and  $k_{p,cir,I}$ .

## VII. OPTIMIZATION AND CONFIGURATION FOR CONTROL PARAMETERS BASED ON MONTE CARLO METHOD

### A. Application of Monte Carlo Method in Control Parameter Optimization

From the results of Sections V and VI, almost all the con-

trol parameters affect the objective function  $OBJ$  and each parameter has a wide feasible range. Meanwhile, different control parameters have different effects on the small-signal stability of the system, i.e., there is no simple monotonic correspondence between control parameters and objective function. Hence, it is not advisable to find the optimal value by traversing the control parameters. Different from deterministic numerical methods, Monte Carlo method solves the non-deterministic (probabilistic or random) mathematical problems through simulating random variables [29].

Table I presents the regions for the control parameters around their initial values, which will be utilized to optimize the control parameters in the following section.

TABLE I  
FEASIBLE REGION OF CONTROL PARAMETERS FOR OPTIMIZATION

Control parameter	Feasible region	Control parameter	Feasible region
$k_{p,R}$	[0.5, 2]	$k_{i,R}$	[100, 250]
$k_{p,PLL,I}$	[1, 50]	$k_{i,PLL,I}$	[10, 200]
$k_{p1,I}$	[0.5, 5]	$k_{i1,I}$	[20, 100]
$k_{p2,I}$	[0.5, 5]	$k_{i2,I}$	[20, 100]
$k_{p3,I}$	[1, 20]	$k_{i3,I}$	[100, 200]
$k_{p4,I}$	[1, 20]	$k_{i4,I}$	[100, 200]
$k_{p,cir,I}$	[0.5, 5]	$k_{i,cir,I}$	[20, 200]

By randomly generating control parameters within the feasible region of Table I, the complex multi-group parameter optimization problems are transformed into computation problems for random numbers and their digital features, thereby simplifying the problem of control parameters adjustment in the optimization process and reducing the complexity. Therefore, the Monte Carlo method is suitable for the optimization and configuration of control parameter for the hybrid LCC-MMC HVDC system.

### B. Optimization and Configuration of Control Parameters Based on Monte Carlo Method

Based on Monte Carlo method, the idea of the algorithm is: ① calculate the value of  $OBJ$  with the initial control parameters of Appendix A Table AI; ② randomly generate a new set of control parameters in the region of Table I, and calculate the new value of  $OBJ$ ; ③ cycle the second step; and ④ choose the optimized parameters with which the  $OBJ$  could reach to a minimum value. The corresponding flow chart is given in Fig. 9. In this figure,  $temp$  is an intermediate variable used to compare  $OBJ$  during the process and the initial value is  $10^{10}$ ;  $k_i$  ( $i = 1, 2, \dots, 14$ ) are the 14 control parameters in Table I;  $k_{\max,i}$  and  $k_{\min,i}$  are the upper and lower limits of the feasible region corresponding to a specific control parameter, respectively;  $n$  ( $0 < n < N_{\max}$ ) is the iteration number and  $N_{\max}$  is set to be 10000;  $J_n$ ,  $D_n$ , and  $OBJ_n$  are the values in the iterative process;  $rand$  is a random number between 0 and 1; and  $k_i^*$  and  $OBJ^*$  are the optimized results.

By conducting the above optimization procedures, the optimized control parameters are obtained as shown in Table II.

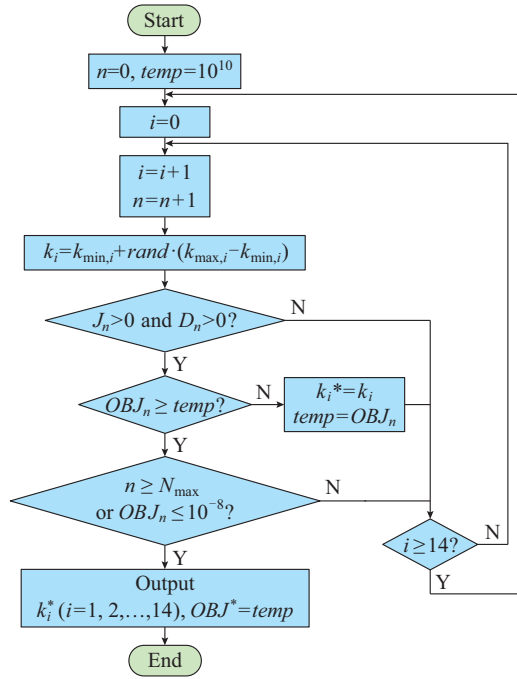


Fig. 9. Flowchart of Monte Carlo method for control parameter optimization.

TABLE II  
OPTIMIZATION RESULTS BASED ON MONTE CARLO METHOD

Control parameter	Optimized value	Original value	Control parameter	Optimized value	Original value
$k_{p,R}$	0.99	0.5	$k_{i,R}$	170.30	200
$k_{p,PLL,I}$	5.25	10.0	$k_{i,PLL,I}$	26.25	50
$k_{p1,I}$	1.77	2.0	$k_{i1,I}$	57.10	50
$k_{p2,I}$	1.07	2.0	$k_{i2,I}$	52.98	50
$k_{p3,I}$	5.75	10.0	$k_{i3,I}$	198.64	125
$k_{p4,I}$	7.09	10.0	$k_{i4,I}$	184.06	125
$k_{p,cir,I}$	1.33	1.0	$k_{i,cir,I}$	134.55	100

### C. Verification of Optimized Control Parameters

The small-signal stability of the hybrid LCC-MMC HVDC system under weak AC grid condition with the optimized control parameters in Table II is compared with that of the initial control parameters of Appendix A Table AI.

Figure 10 presents the comparison of  $OBJ$  before and after the optimization when  $SCR_2$  varying from 1.1 to 2.0. The root locus of hybrid system after the optimization when  $SCR_2$  decreasing from 2.0 to 1.1 is presented in Fig. 11. As shown in Figs. 10 and 3, with the initial control parameters, the  $OBJ$  value becomes negative and the locus moves to right-half plane when  $SCR_2$  is smaller than 1.27. However, as shown in Figs. 10 and 11, after optimization, the  $OBJ$  value remains positive and the locus is always in the left-half plane even when  $SCR_2 = 1.1$ , which means that the small-signal stability of the system is greatly enhanced under weak AC grid condition with the optimized control parameters.

Figure 12 shows the time-domain response of the hybrid system from PSCAD/EMTDC when  $SCR_2 = 1.1$ . When  $t = 6$  s,  $U_{dc,ref,I}$  step-changes from 1.0 p.u. to 1.05 p.u.. The response

of DC voltage  $U_{dc,I}$  at MMC side with optimized control parameter is shown in Fig. 12.

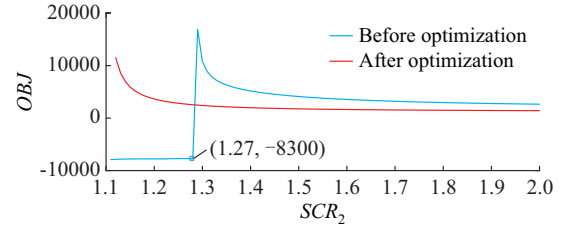


Fig. 10. Comparison of  $OBJ$  before and after optimization when  $SCR_2$  varying from 1.1 to 2.0.

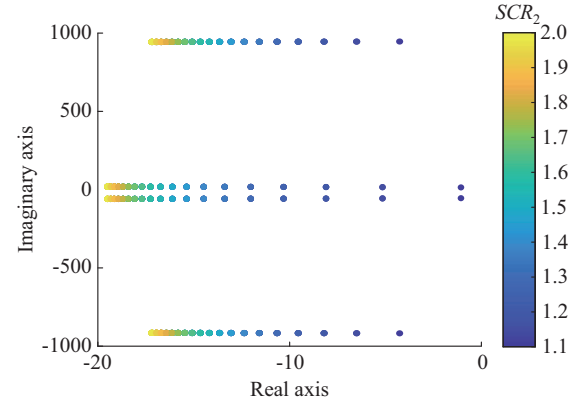


Fig. 11. Root locus of hybrid system after optimization when  $SCR_2$  decreasing from 2.0 to 1.1.

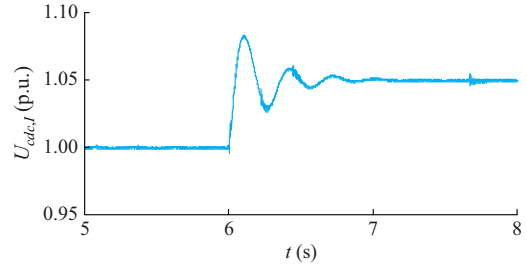


Fig. 12. Response of  $U_{dc,I}$  when  $U_{dc,ref,I}$  step-changes with optimized parameters.

It can be observed from Fig. 12 that after the optimization, the system can successfully operate and has a satisfactory dynamic response characteristic when connected to the extremely weak AC grid ( $SCR_2 = 1.1$ ). Figure 13 shows the time-domain comparison from PSCAD/EMTDC at the operation point of  $SCR_1 = 2.5$ ,  $SCR_2 = 1.3$ ,  $I_{dc,ref,R} = 1.0$  p.u.,  $U_{dc,ref,I} = 1.0$  p.u., and  $U_{i,ref,I} = 1.0$  p.u.. Initially,  $SCR_2$  is 1.30; when  $t = 5$  s,  $SCR_2$  is changed to 1.25. The DC current  $I_{dc,R}$  at LCC side and the DC voltage  $U_{dc,I}$  at MMC side are shown in Fig. 13.

From the simulation results of Fig. 13, with the optimized control parameters, the system can keep stable when  $SCR_2$  decreases to 1.25, i.e., the optimized control parameters can enhance the small-signal stability of the system under weak AC grid conditions. However, the system with the initial control parameters experiences the instability when  $SCR_2$  decreases to 1.25. For further validation, the comparison of dynamic and fault recovery characteristics before and after parameter optimization in PSCAD/EMTDC is shown in Fig. 14.

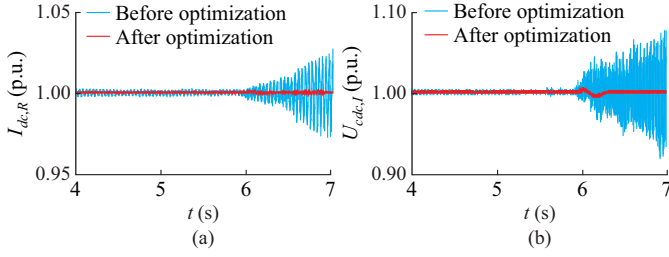


Fig. 13. Time-domain comparison before and after optimization from PSCAD/EMTDC. (a) DC current at LCC side. (b) DC voltage at MMC side.

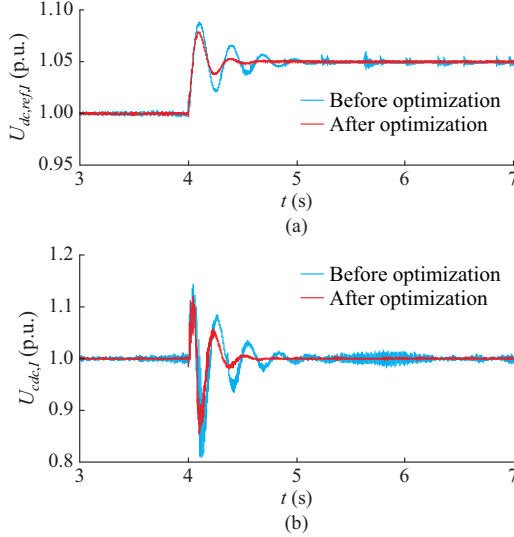


Fig. 14. Comparison of dynamic and fault recovery characteristics before and after parameter optimization in PSCAD/EMTDC. (a) DC voltage responses when  $U_{dc,ref,I}$  step-changes. (b) DC voltage response to single-phase fault.

When connected to weak AC grid ( $SCR_2 = 1.3$ ) and  $t = 4$  s,  $U_{dc,ref,I}$  step-changes from 1.0 p.u. to 1.05 p.u.. With the optimized parameters, it can be observed from Fig. 14(a) that the overshoot and the setting time are both reduced, and the low-frequency oscillation is also well damped. As shown in Fig. 14(b), when connected to the weak AC grid, the optimized control parameters can improve the fault recovery performance of the system.

## VIII. CONCLUSION

To enhance the small-signal stability and dynamic response characteristic of the hybrid LCC-MMC HVDC system under weak AC grid condition, an objective function is developed considering the quadratic index and damping ratio characteristics of the hybrid system. And all the control parameters of LCC and MMC are optimized by Monte Carlo method. Then, the following conclusions can be obtained.

1) The strength of AC grid has a significant effect on the small-signal stability of the system, especially under weak AC grid condition with the initial control parameters.

2) Based on the participation factor and parametric sensitivity analysis, the key control parameters that have major impact on the small-signal stability of the system are identified, which are the constant DC current controller gain of

LCC, reactive power outer-loop gain of MMC,  $d$ -axis and  $q$ -axis inner-loop gains of MMC, and the CCSC gain.

3) Based on the derived objective function and Monte Carlo method, the control parameters are optimized with the objective function reaching to a minimum value. The eigenvalue results and detailed electromagnetic transient (EMT) simulation results show that the optimized control parameters can greatly enhance the small-signal stability of the system under weak AC grid condition.

4) The comparison and verification of EMT show that the optimization method proposed in this paper can enhance the small-signal stability, dynamic responses and even fault recovery performance of the hybrid LCC-MMC HVDC system when connected to a weak AC grid.

## APPENDIX A

TABLE AI  
PARAMETERS OF HYBRID LCC-MMC HVDC SYSTEM

Scenario	Physical meaning	Value
LCC station	Rated capacity	$P_{dN,R} = 1000$ MW
	Rated voltage	$V_{sN,R} = 230$ kV
	SCR at LCC side	$SCR_1 = 2.5$
	AC system impedance	$Z_{s,R} = 21.16 \Omega$ ( $Z_{s,R} = U_{sN,R}^2 / P_{dN,R} / SCR_1$ )
	Rated AC voltage	$U_{t,R} = 1$ p.u.
	Converter reactance	$X_{t,R} = 0.18$ p.u.
	Reference angular frequency	$\omega_0 = 314.16$ rad/s
	PLL1	$k_{p,PLL,R} = 10, k_{i,PLL,R} = 50$
LCC control system	DC current controllers	$k_{p,R} = 0.5, k_{i,R} = 200$
	Filter time constant	$T_{m,L,dc} = 5$ ms
	Rated capacity	1000 MW
MMC station	Rated voltage	$V_{sN,I} = 230$ V
	SCR at MMC side	$SCR_2 = 2$
	AC system impedance	$Z_{s,I} = 26.45 \Omega$ ( $Z_{s,I} = U_{sN,I}^2 / P_{dN,I} / SCR_2$ )
	Rated AC voltage	$U_{t,I} = 1$ p.u.
	Converter reactance	$X_{t,I} = 0.15$ p.u.
	Number of modules	200
	Capacitor size in module	10 mF
	Bridge arm inductance	$L_{arm} = 0.055$ H
MMC control system	PLL2	$k_{p,PLL,I} = 10, k_{i,PLL,I} = 50$
	DC voltage controller	$k_{p1,I} = 2, k_{i1,I} = 50$
	AC voltage controller	$k_{p2,I} = 2, k_{i2,I} = 50$
	$d$ -axis inner-loop controller	$k_{p3,I} = 10, k_{i3,I} = 125$
	$q$ -axis inner-loop controller	$k_{p4,I} = 10, k_{i4,I} = 125$
	CCSC	$k_{p,cir,I} = 1, k_{i,cir,I} = 100$
	Filter time constant	$T_{m,ud} = T_{m,uq} = 1$ ms
	Filter time constant	$T_{m,id} = T_{m,iq} = 0.1$ ms
DC system	Rated capacity	500 kV, 2 kA
	Smoothing reactor	$L_{dc,R} = 0.3$ H
Overhead line at DC side	Resistance at LCC side and MMC side	$R_{oh,R} = R_{oh,I} = 6.35 \Omega$
	Inductance at LCC side and MMC side	$L_{oh,R} = L_{oh,I} = 0.88$ mH
	Capacitance per kilometer	$C_{oh} = 0.013$ $\mu$ F

TABLE AII  
STATE VARIABLES OF HYBRID LCC-MMC HVDC SYSTEM

Sub-system	Physical meaning	Variable
AC system 1	Voltage of point of common coupling (PCC) in rectifier station	$U_{id,R}, U_{iq,R}$
	Voltage and current of AC filters	$U_{cr2d,R}, U_{cr2q,R},$ $U_{cr3d,R}, U_{cr3q,R},$ $U_{cr4d,R}, U_{cr4q,R},$ $I_{Lr1d,R}, I_{Lr1q,R},$ $I_{Lr2d,R}, I_{Lr2q,R}$
		AC current
		$I_{sd,R}, I_{sq,R}$
	DC current controller	$x_{1,R}, I_{dcm,R}, I_{dc,R}$
LCC control	Stage variable of PLL1	$x_{2,R}, x_{PLL,R}$
	Angular frequency and phase of PLL1	$\omega_1, \theta_1$
	Delay trigger angle and advance trigger angle	$\alpha, \beta$
AC system 2	Voltage of PCC in inverter station	$U_{id,I}, U_{iq,I}$
	AC current	$I_{sd,I}, I_{sq,I}$
MMC station	DC component of SM capacitor voltage	$U_{cdc,I}$
	Fundamental frequency component of SM capacitor voltage	$u_{cRd,I}, u_{cRq,I}$
	Second harmonic component of SM capacitor voltage	$u_{cId,I}, u_{cIq,I}$
	Third harmonic component of SM capacitor voltage	$u_{c3x,I}, u_{c3y,I}$
	Fundamental current of bridge arm	$I_{sd,I}, I_{sq,I}$
	Second-order circulating current	$I_{cirId,I}, I_{cirIq,I}$
	DC voltage of MMC	$U_{dc,I}$
	DC current of MMC	$I_{dc,I}$
	Measured voltage of PCC in inverter station	$U_{idm,I}, U_{iqm,I}$
	Measured AC current	$I_{sdm,I}, I_{sqm,I}$
MMC control	d-axis inner-loop control	$x_{1,I}$
	q-axis inner-loop control	$x_{2,I}$
	DC voltage control	$x_{3,I}$
	AC voltage control	$x_{4,I}$
	d-axis control of CCSC	$f_{1,I}$
	q-axis control of CCSC	$f_{2,I}$
	Stage variable of PLL2	$x_{5,I}, x_{PLL,I}$
	Angular frequency and phase of PLL2	$\omega_2, \theta_2$
DC system	DC line capacitor voltage	$U_{cdc}$
	DC line current	$I_{dc,R}$

## REFERENCES

- [1] C. Guo, Y. Zhang, A. M. Gole *et al.*, "Analysis of dual-infeed HVDC with LCC-HVDC and VSC-HVDC," *IEEE Transactions on Power Delivery*, vol. 27, no. 3, pp. 1529-1537, Jul. 2012.
- [2] E. Rahimi, A. M. Gole, J. B. Davies *et al.*, "Commutation failure analysis in multi-infeed HVDC systems," *IEEE Transactions on Power Delivery*, vol. 26, no. 1, pp. 378-384, Jan. 2011.
- [3] O. B. Nayak, A. M. Gole, D. G. Chapman *et al.*, "Dynamic performance of static and synchronous compensators at an HVDC inverter bus in a very weak AC system," *IEEE Transactions on Power Systems*, vol. 9, no. 3, pp. 1350-1358, Aug. 1994.
- [4] C. V. Thio, J. B. Davies, and K. L. Kent, "Commutation failures in HVDC transmission systems," *IEEE Transactions on Power Delivery*, vol. 11, no. 2, pp. 946-957, Apr. 1996.
- [5] A. Zheng, C. Guo, P. Cui *et al.*, "Comparative study on small-signal stability of LCC-HVDC system with different control strategies at the inverter station," *IEEE Access*, vol. 7, pp. 34946-34953, Mar. 2019.
- [6] C. Guo, Z. Yin, and C. Zhao, "Small-signal dynamics of hybrid LCC-VSC HVDC systems," *International Journal of Electrical Power & Energy Systems*, vol. 98, pp. 362-372, Jun. 2018.
- [7] A. Lesnicar and R. Marquardt, "An innovative modular multilevel converter topology suitable for a wide power range," in *Proceedings of 2003 IEEE Bologna Power Tech Conference*, Bologna, Italy, Jun. 2003, pp. 1-6.
- [8] M. Hagiwara and H. Akagi, "Control and experiment of pulsewidth-modulated modular multilevel converters," *IEEE Transactions on Power Electronics*, vol. 24, no. 7, pp. 1737-1746, Jul. 2009.
- [9] M. Saeedifard and R. Irvani, "Dynamic performance of a modular multilevel back-to-back HVDC system," *IEEE Transactions on Power Delivery*, vol. 25, no. 4, pp. 2903-2912, Oct. 2010.
- [10] S. Debnath, J. Qin, B. Bahrani *et al.*, "Operation, control, and applications of the modular multilevel converter: a review," *IEEE Transactions on Power Electronics*, vol. 30, no. 1, pp. 37-53, Jan. 2015.
- [11] C. Guo, C. Zhao, A. Montanari *et al.*, "Characteristics of hybrid bipolar HVDC transmission system," *Proceedings of the CSEE*, vol. 32, no. 2, pp. 98-104, Apr. 2012.
- [12] H. Rao, C. Hong, B. Zhou *et al.*, "Study on the improvement of the centralized feeding problem of flexible DC to multi-DC in the receiving end of Wudong Dete high-voltage multi-terminal DC project," *Southern Power System Technology*, vol. 11, no. 3, pp. 1-5, May 2017.
- [13] Z. Zhang, Z. Xu, Y. Xue *et al.*, "DC-side harmonic currents calculation and DC-loop resonance analysis for an LCC-MMC hybrid HVDC transmission system," *IEEE Transactions on Power Delivery*, vol. 30, no. 2, pp. 642-651, Apr. 2015.
- [14] G. Li, J. Liang, T. Joseph *et al.*, "Feasibility and reliability analysis of LCC DC grids and LCC/VSC hybrid DC grids," *IEEE Access*, vol. 7, pp. 22445-22456, Feb. 2019.
- [15] Y. Xue, F. Ge, Z. Zhao *et al.*, "Control strategy for hybrid LCC-C-MMC HVDC system under AC fault at rectifier side," *The Journal of Engineering*, vol. 2019, no. 16, pp. 3259-3263, Mar. 2019.
- [16] D. Xing, J. Su, D. Hu *et al.*, "Solution to reduce voltage stress of submodule in LCC-MMC transmission system at the condition of communication fault," *The Journal of Engineering*, vol. 2019, no. 16, pp. 1873-1876, Mar. 2019.
- [17] N. M. Haleem, A. D. Rajapakse, A. M. Gole *et al.*, "Investigation of fault ride-through capability of hybrid VSC-LCC multi-terminal HVDC transmission systems," *IEEE Transactions on Power Delivery*, vol. 34, no. 1, pp. 241-250, Feb. 2019.
- [18] B. Lou, H. Zhou, Z. Xu *et al.*, "Fault response comparison of LCC-MMC hybrid topologies and conventional HVDC topology," *The Journal of Engineering*, vol. 2019, no. 16, pp. 2068-2073, Mar. 2019.
- [19] O. Kotba, M. Ghandharia, R. Eriksson *et al.*, "On small signal stability of an AC/DC power system with a hybrid MTDC network," *Electric Power Systems Research*, vol. 136, pp. 79-88, Feb. 2016.
- [20] C. Guo, Z. Yin, Y. Wang *et al.*, "Investigation on small-signal stability of hybrid LCC-MMC HVDC system," *Proceedings of the CSEE*, vol. 39, no. 4, pp. 1040-1052, Apr. 2019.
- [21] J. Lyu, X. Cai, and M. Molinas, "Optimal design of controller parameters for improving the stability of MMC-HVDC for wind farm integration," *IEEE Journal of Emerging and Selected Topics in Power Electronics*, vol. 6, no. 1, pp. 40-53, Mar. 2018.
- [22] J. Lin, G. Li, Y. Sun *et al.*, "Small-signal analysis and control system parameter optimization for DFIG wind turbines," *Automation of Electric Power Systems*, vol. 33, no. 5, pp. 86-90, Mar. 2009.
- [23] C. Zhang, W. Wang, G. He *et al.*, "Analysis of sub-synchronous oscillation of full-converter wind farm based on sequence impedance and an optimized design method for PLL parameters," *Proceedings of the CSEE*, vol. 37, no. 23, pp. 6757-6767, Oct. 2017.
- [24] M. Szechtman, T. Wess, and C. V. Thio, "A benchmark model for HVDC system studies," in *Proceedings of International Conference on AC and DC Power Transmission*, London, UK, Sept. 1991, pp. 374-378.
- [25] Q. Peng, C. Ma, X. Yang *et al.*, "Participation factors and contribution factors in linear modal analysis," *Power System Technology*, vol. 34, no. 2, pp. 92-96, Feb. 2010.
- [26] S. Jiang, A. M. Gole, U. D. Annakkage *et al.*, "Damping performance analysis of IPFC and UPFC controllers using validated small-signal models," *IEEE Transactions on Power Delivery*, vol. 26, no. 1, pp. 446-454, Jan. 2011.
- [27] X. Duan, J. Yuan, Y. He *et al.*, "Sensitivity analysis methods on voltage stability of electric power systems," *Automation of Electric Power*

*Systems*, vol. 21, no. 4, pp. 9-12, Apr. 1997.

- [28] V. Radisavljevic and S. Koskie, "Suboptimal strategy for the finite-time linear-quadratic optimal control problem," *IET Control Theory & Applications*, vol. 6, no. 10, pp. 1516-1521, Jul. 2012.
- [29] B. Vo, S. Singh, and A. Doucet, "Sequential Monte Carlo methods for multitarget filtering with random finite sets," *IEEE Transactions on Aerospace and Electronic Systems*, vol. 41, no. 4, pp. 1224-1245, Oct. 2005.

**Chunyi Guo** received the B.S. and Ph.D. degrees in power system and automation from North China Electric Power University (NCEPU), Beijing, China, in 2007 and 2012, respectively. He is currently an Associate Professor at NCEPU. His research interests include HVDC and power electronics.

**Peng Cui** received the B.S. degree from North China Electric Power University (NCEPU), Beijing, China, in 2014. Currently, he is pursuing the M.S. degree in power system and automation from NCEPU. His research interests include HVDC and power electronics.

**Chengyong Zhao** received the B.S., M.S., and Ph.D. degrees in power system and its automation from North China Electrical Power University (NCEPU), Beijing, China, in 1988, 1993, and 2001, respectively. Currently, he is the Deputy Director of the Flexible Transmission and Distribution Institute, Electrical and Electronic Engineering School, NCEPU. His research interests include HVDC, flexible AC transmission systems, and power quality.